Tellus (1988), *40B*, 358–379

Three-dimensional modeling of transport of chemical species from continents to the Atlantic Ocean

By R. A. BROST, R. B. CHATFIELD, J. P. GREENBERG, P. L. HAAGENSON, B. G. HEIKES, S. MADRONICH, B. A. RIDLEY and P. R. ZIMMERMAN, *National Center for Atmospheric Research*, P.O. Box 3000, Boulder, Colorado 80307, USA*

(Manuscript received 3 November 1987; in final form 18 May 1988)

ABSTRACT

A three-dimensional, Eulerian modeling system was used to study transport of chemical species from North America and Europe to the Atlantic Ocean. A mesoscale meteorological model simulated April 1982 with 10 consecutive 3-day runs. This simulated meteorology drove a chemical model with 24 predicted and transported species, and 11 non-transported (photochemical equilibrium) species. We used artificially clean initial and boundary conditions to investigate the effect of anthropogenic emissions on ozone. Two weeks were needed to "spin up" the chemical model. At individual times, plumes were intermittently found moving out over the ocean from the continental source region. In the planetary boundary layer, the time-average plumes were significantly weakened by vertical transport and aqueous chemistry in clouds. The continental plume of Europe was often more persistent than that from North America. The simulated total fluxes of sulfur (S) and nitrogen (N) from North America to the Atlantic Ocean, in a layer from the surface to 5.5 km high, were in reasonable agreement with data analyses. The eastward, atmospheric flux of S was 4.8 Tg/yr and that of N was 1.8 Tg/yr.

1. Introduction

There are several important reasons to study the transport of atmospheric trace species from continents of the northern hemisphere to oceans and continents downwind. Anthropogenically emitted nitrogen oxides (NO_x) and hydrocarbons drive photochemical reactions producing ozone (O_3), which then blends into the hemispheric ozone background. Large portions of the cycles of nitrogen (N), sulfur (S), and carbon (C) species, from source to deposition, are completed in this continent to ocean scale, and thus may contribute to the flux of trace species into the oceans. Many chemical, physical, and meteorological processes interact in this flux.

This work focuses on transformation and transport from North America and Europe to the remote Atlantic Ocean. We also examine the importance of clouds, i.e., vertical transport and aqueous chemistry. We were partly motivated by the need to develop modeling expertise to accompany the Air/Ocean Chemistry Experiment (AEROCE). This is an exploratory study in an ongoing effort.

We used an Eulerian modeling system developed at the National Center for Atmospheric Research (NCAR) and described in Chang (1985, 1986), and Chang et al. (1987). The system includes the mesoscale meteorological model of Anthes and Warner (1978) and the regional chemical model of Chang et al. (1987). The largest previous published use of the chemical model had a horizontal scale of 2,400 km. We have increased the spatial scale to 12,000 km, and the time scale from 3 days to 1 month. We refer to this scale as synoptic, because it is intermediate in space and time between regional and global

* The National Center for Atmospheric Research is sponsored by the National Science Foundation, Atmospheric Chemistry Division, reference 1905-88-1.

models. We do not know any time dependent study on this scale explicitly describing both photochemistry and transport.

Many spatial and temporal scales exist in models of atmospheric chemistry. The model shifts from detailed chemistry to detailed transport as the spatial dimensionality increases. A zero-dimensional model is almost pure chemistry, with at most dilution representing turbulent mixing, and changes in temperature and pressure representing mean transport. In three-dimensional modeling, the strength is the transport by grid-resolved circulations and the weakness is the limited number of species and reactions that can be considered. The main difficulties are computational time and storage. Even a three-dimensional model has substantial vertical transport by subgrid-scale motions, but it resolves more vertical motions than a model with fewer dimensions. Likewise, our chemistry resolves nitrogen oxides but parameterizes hydrocarbon oxidation.

It is important to develop expertise in three-dimensional Eulerian modeling of chemical trace species (Duce et al., 1984). We need to determine what chemical questions are answerable in models that are limited in spatial extent (i.e., less than global). We also need to know whether we can simulate realistic concentrations. Furthermore, how do the spatial and temporal scale of the model and the temporal scale of the chemistry determine whether the concentrations are affected by boundary conditions, initial conditions, and meteorology (Brost, 1988)?

Regional-scale modeling has used smaller spatial scales than our synoptic-scale model, but about the same number of chemical species (Carmichael et al., 1984a, b; Lamb, 1982, 1983, 1985; McRae et al., 1982, 1983; van Dop and DeHaan, 1983; Venkatram and Karamchandani, 1986; Chang et al., 1987).

Global-scale work involved tracers or simple chemistry, and used meteorology from a general circulation model (GCM). Mahlman and Moxim (1978) studied tracer evolution from an instantaneous midlatitude source. Mahlman et al. (1980) did tracer experiments with ozone precursors. Levy et al. (1982) transported tropospheric nitrous oxide (N_2O), and Levy et al. (1985) simulated chemically conserved O_3 with a stratospheric source and a surface sink. Nuclear winter studies had interactive transport, radiation, and scavenging (Malone et al., 1986). Prather et al. (1987) studied fluorocarbons as tracers of atmospheric motions, and Jacob et al. (1987) studied sources and transport of krypton, 85.

2. Modeling system

2.1. Meteorology

We simulated the meteorology of April 1982 using 10 consecutive runs of 3-day duration with the mesoscale model of Anthes and Warner (1978). We chose this April because of the meteorological data available at NCAR and because of the many storms over the eastern United States. We used simulated rather than observed meteorology because the temporal resolution was higher and the spatial coverage of precipitation data was more complete, especially over the ocean. Each run, however, started from observed meteorology. The advantage of 3-day runs was that we indeed simulated this particular month. If we had done a single run for one month, after 7–10 days of simulation there would have been no correspondence between the simulated and actual meteorology. A single one-month run would have produced, at best, a climatological spring month. After 3 days, each model simulation departed from observations, so we returned to the observed state of the atmosphere every third day. These changes caused no apparent difficulty for the stability of chemical integrations. The 3-day period was customary with the mesoscale model (Anthes et al., 1987). 3 days also seemed a reasonable compromise between the magnitude of simulation errors and the practical difficulties associated with additional computer runs. This kind of meteorology will in later papers allow detailed comparison of simulated and observed chemistry for individual episodes or combined episodes for up to several months. Climatological meteorology, for example, from a GCM, would not allow such detailed comparison.

We used the version of the mesoscale model with the high resolution planetary boundary layer (PBL) model described in Anthes et al. (1987). This PBL parameterization was adapted from Blackadar (1976, 1979), and tested in Zhang and Anthes (1982). The grid had 46 points north-south, 61 east-west, and 15 in the vertical, for a

total of 42,000 grid points. The nominal horizontal resolution was $\Delta x = \Delta y = 190$ km. The domain size was about 12,000 × 9,000 km.

The vertical coordinate for both models was $\sigma = (P - P_{top})/P^*$. The pressure P was at the height where σ was evaluated. The pressure at the top of the model $P_{top} = 100$ mb, $P^* = P_{surf} - P_{top}$, and P_{surf} was the surface pressure. The vertical resolution was variable. The boundaries between vertical layers were about 0, 80 m, 160 m, 290 m, 500 m, 800 m, 1400 m, 2 km, 2.7 km, 3.8 km, 4.9 km, 6.2 km, 7.7 km, 9.4 km, 11.8 km, and 16 km above sea level.

The meteorological model used a time step of 285 s, and we saved simulated meteorology at 6-h intervals. The variables archived were three-dimensional fields of horizontal winds (u, v), temperature T, and water vapor mixing ratio Q_v. We also saved two-dimensional fields of surface pressure, total rain, and ground temperature T_g. The chemical model used these meteorological fields to diagnose precipitating and nonprecipitating cloudiness, vertical velocity, and vertical eddy diffusivity K_z (in the PBL).

Fig. 1a shows the 190-km resolution, smoothed terrain. Greenland was the highest feature because the grid could not resolve the peaks of the Rocky Mountains. Fig. 1b gives the observed water vapor mixing ratio Q_v at the start of the second 3-day run, for height $z = 80$–160 m. The air was dry over Canada, Alaska, Greenland, and the Sahara. Moisture pushed north over the Atlantic Ocean and Europe. Over the Atlantic Ocean, individual storms caused north-south excursions of the 5 g/kg isoline, which also suggested the movement of the polar front. The maximum simulated precipitation for April occurred just off the east coast of North America where cold continental air encountered the warm Gulf Stream (Fig. 1c). Other precipitation maxima were less important for the vertical transport of pollutants from North America.

For the same meteorology, domain, and modeling system, Brost and Chatfield (1988) simulated radon, which is chemically inert and is not scavenged by droplets. The surface of the earth emits radon at a well-known rate, and radon does not deposit on the surface. Because radon decays radioactively with an exponential decay time of 5.51 days, radon concentrations are large near the surface over continents, decrease with height above the continents, and decrease with distance moving out over the ocean. Thus, modeling radon tests horizontal and vertical transport in a 3-dimensional model. Brost and Chatfield compared the rising motion before individual cold

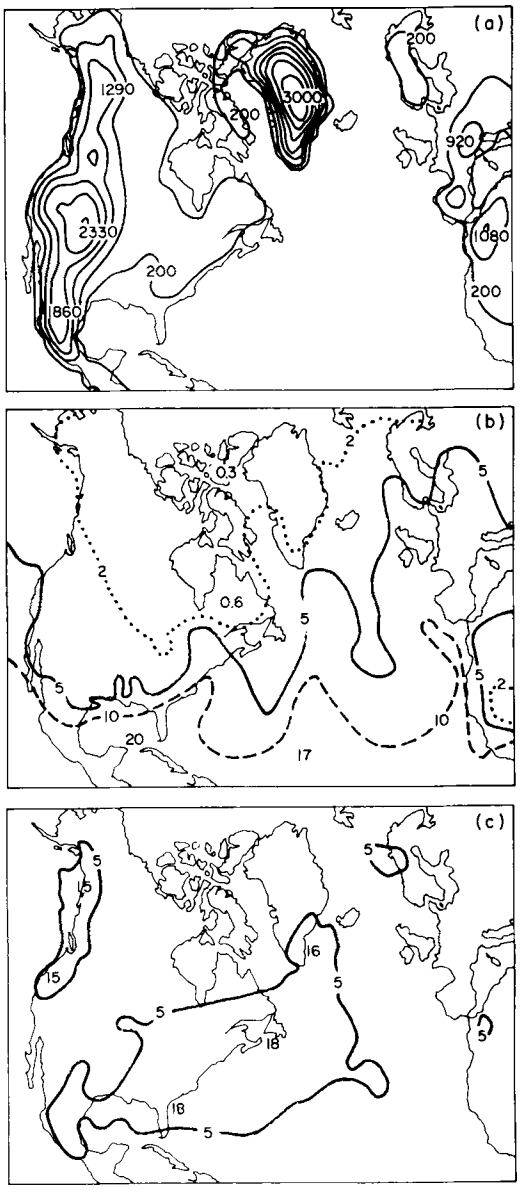

Fig. 1. Panel (a) is the smoothed terrain height ASL in meters. Panel (b) is the observed water vapor mixing ratio Q_v (g/kg) at 00 GMT on 4 April 1982. Panel (c) is the model-simulated total rain in centimeters for April 1982.

fronts with the radon concentration aloft. They showed how well transport associated with individual weather events was resolved by this model and grid resolution.

2.2. Chemical transport model

2.2.1. Equations. We based our regional chemical model on Chang (1985, 1986) and Chang et al. (1987). The chemical model used the vertical and horizontal structure of the mesoscale model of Anthes and Warner (1978), with some minor differences (Chang et al., 1987).

The equation solved for the concentration of chemicals was

$$\frac{\partial C^*}{\partial t} = -m^2\left\{\frac{\partial}{\partial x}\left(\frac{uC^*}{m}\right)+\frac{\partial}{\partial y}\left(\frac{vC^*}{m}\right)\right\}-\frac{\partial \dot{\sigma} C^*}{\partial \sigma} + \left(\frac{g}{P^*}\right)^2\frac{\partial}{\partial \sigma}\left(\rho^2 K_z\frac{\partial C^*}{\partial \sigma}\right)+\left(\frac{\partial C^*}{\partial t}\right)_{\text{chem}} + \left(\frac{\partial C^*}{\partial t}\right)_{\text{cloud}}. \quad (1)$$

Here $C^* = CP^*$, and C is the trace species mixing ratio. The map scale factor m is the ratio of the transformed distance on the Lambert conformal map projection to the true distance. The velocities in the (x, y, σ) directions are $(u, v, \dot{\sigma})$. The acceleration of gravity is g, and ρ the density of air. The last two terms in (1) are the temporal changes by chemistry (including emissions) and by clouds.

The time step for advection and diffusion was 20 min; that for the gas-phase chemistry was variable with a maximum of 20 min; and that for clouds was 1 h. The chemical model had a ratio of 50–60 to 1 simulated time to CPU time on one processor of the CRAY XMP-4800. A month simulation needed 12–15 h of CPU time. The simulated meteorological variables, u, v, and P^*, were archived at 6-h intervals and were interpolated linearly to each time step at 20-min intervals. The mass continuity equation specified vertical velocity.

For a smaller domain, Brost (1988) found that the simulated atmospheric chemical concentrations were sensitive to initial conditions, boundary conditions, and meteorology. It remains to be determined in detail which of the concentrations in the current large domain are sensitive to these. An informed guess is that as the horizontal domain and the length of simulation grow, chemistry with slower time scales becomes important. Thus, chemistry becomes more important compared with initial conditions and boundary conditions. Throughout the domain, concentrations may continue to be sensitive to meteorology.

2.2.2. Advection scheme. The iterated upstream finite difference scheme of Smolarkiewicz (1983, 1984) was used for advection. The scheme has been used in a cloud model by Smolarkiewicz and Clark (1986) and in a regional chemical model by Chang et al. (1987). This scheme conserved the chemical mass well, maintained positivity of the chemical concentration, did not create maxima and minima when none previously existed, was computationally efficient, and only required one permanent storage location per grid cell for each chemical (Chang et al., 1987). Spatial smoothing of the emissions and temporal averaging of the simulated concentrations improved the forecast. A 5×5 source array or advected shape was resolved well (Brost et al., 1988a). The simulation of emissions or blobs of concentration on smaller spatial scales is not particularly important here.

2.2.3. Vertical subgrid-scale turbulent diffusion. The vertical turbulence parameterization in Brost et al. (1988a, b) was used in the chemical model. For the unstable PBL, the vertical eddy diffusivity was given by

$$K_z = w_* h\frac{z}{h}\left(1-\frac{z}{h}\right). \quad (2)$$

The convective velocity scale

$$w_* = (\overline{w' T_{v0}'} h g/T_0)^{1/3},$$

with T_0 a reference temperature, $\overline{w' T_{v0}'}$ was the surface vertical turbulent flux of virtual potential temperature, and h was the height of the unstable PBL (Brost et al., 1988a, b; Wyngaard and Brost, 1984; Moeng and Wyngaard, 1984). Following Brost and Wyngaard (1978), for the neutral and stable PBL the eddy diffusivity was

$$K_z = \frac{k u_* h(1-z/h)^{1.5}}{(1+4.7(z/h)(h/L))}, \quad (3)$$

where the von Karman constant $k = 0.35$, u_* is the friction velocity, and h is here the depth of the stable or neutral boundary layer, taken from the diagnostic equations given in Brost et al. (1988a). The surface fluxes of heat and momentum were calculated following Businger et al.

(1971). The finite difference scheme for diffusion was fully implicit (Richtmyer, 1957).

2.2.4. Cloud parameterization. Precipitating clouds existed when the mesoscale model simulated more than 0.01 cm/h of rain. The rainfall rate determined the cloud cover (Walcek and Taylor, 1986). The Anthes et al. (1987) parameterization diagnosed the coverage of nonprecipitating clouds. The parameterization of Walcek and Taylor (1986) vertically redistributed chemicals in precipitating and nonprecipitating clouds. Both kinds of clouds used the aqueous chemistry presented in Walcek and Taylor (1986), and modified to be zero-dimensional in Chang et al. (1987).

2.2.5. Gas-phase chemistry. We used the gas-phase mechanism of Stockwell (1986) as carried out in Chang et al. (1987). Table 1 summarizes the chemical species in the model. There were 24 predicted and transported species, including O_3, nitric oxide (NO), nitrogen dioxide (NO_2), nitrogen trioxide (NO_3), dinitrogen pentoxide (N_2O_5), nitric acid (HNO_3), peroxyacetyl nitrate (PAN), hydrogen peroxide (H_2O_2), two other peroxides, formaldehyde (HCHO), acetaldehyde, carbon monoxide (CO), organic acid, ethane, other alkanes, three olefins, two aromatics, sulfur dioxide (SO_2), sulfate (SO_4^{2-}), and ammonia (NH_3). There were 11 non-transported species, including hydroxyl (HO) and hydroperoxy radical (HO_2). (For these species, the time derivatives were set to zero and the algebraic set was solved iteratively for the concentrations at that time and location.) The solver was an explicit, two-step method.

2.2.6. Photolysis rate constants. Actinic fluxes were calculated with the delta-Eddington approach of Joseph et al. (1976). Details and databases were given in Chang et al. (1987). The photolysis rate constants in clear (noncloudy) air varied with latitude, height, and hour angle. We saved the calculations at 6 heights (0, 2, 6, 10, 15, 20 km), 13 times (13-h angles from local noon to local midnight), and 10 latitudes (from 0–90° N in 10° increments). Clouds may substantially modify the clear air photolysis rate constants (Madronich, 1987). We adjusted the clear air values for cloud cover following Chang et al. (1987). The archived values were linearly interpolated to local height, hour angle, and latitude.

2.2.7. Emissions. We used only anthropogenic

Table 1. *Chemical species and associated physical properties in model*

Species name	Dry deposition surface resistance[1] land	water	Emitted (x)
	Transported species		
sulfur dioxide (SO_2)	R_s	R_s	x
sulfuric acid (H_2SO_4)	see note [2] below		x
nitric oxide (NO)	R_s	500	x
nitrogen dioxide (NO_2)	R_s	500	x
nitrogen trioxide (NO_3)	—	—	
dinitrogen pentoxide (N_2O_5)	—	—	
nitric acid (HNO_3)	0.0	0.0	
peroxyacetyl nitrate (PAN)	—	—	
ammonia (NH_3)	0.2 R_s	0.2 R_s	x
ozone (O_3)	0.6 R_s	2000	
hydrogen peroxide (H_2O_2)	0.1 R_s	0.1 R_s	
carbon monoxide (CO)	—	—	x
formaldehyde (HCHO)	0.5 R_s	0.5 R_s	x
aldehydes	2.0 R_s	2.0 R_s	x
organic acid	R_s	R_s	x
organic peroxide	0.3 R_s	0.3 R_s	
peroxyacetic acid	0.3 R_s	0.3 R_s	
butane + other alkanes	—	—	x
ethane	—	—	x
ethene (C_2)	—	—	x
propene (C_3)	—	—	x
butene + other reactive olefins	—	—	x
toluene	—	—	x
xylene	—	—	x
	Non-transported species		
hydroxyl (HO)			
hydroperoxy radical (HO_2)			
oxygen singlet-D			
acetyl peroxy radical			
methyl peroxy radical			
HO-ethylene peroxy radical			
HO-propylene peroxy radical			
HO-higher olefin peroxy radical			
alkyl peroxy radical			
Criegee intermediate (C_1)			
Criegee intermediate (C_2)			
	Additional species		
water vapor (H_2O)	(specified from meteorological data)		
methane (CH_4)	(1.7 ppm)		

[1] Only some species are emitted and dry deposited. Surface resistance is in s m^{-1}. R_s is SO_2 surface resistance, tabulated as a function of land type, season, insolation, and surface wetness (Walcek et al., 1986). Dash (—) shows that the species is not dry deposited.

[2] Sulfate surface resistance is computed from meteorology (Walcek et al., 1986).

emissions. We intend to include natural emissions in future work, and show the effect on the ozone concentrations and budgets. Here the resulting simulations necessarily show some unrealistic behavior, but they do highlight anthropogenic effects. We used data for $SO_x = SO_2 + SO_4^{2-}$, NO_x, reactive hydrocarbons, and NH_3 (Table 2). For the United States, emissions came from the National Acid Precipitation Assessment Program (NAPAP, see Toothman et al., 1984 and Middleton, 1987). In Canada, the emissions were from Voldner et al. (1980). The European emissions were for European Russia, and western and eastern Europe (Fig. 1). In Europe, we used industry sources (unpublished) and Hov et al. (1986) for SO_x, NO_x, and hydrocarbons. European NH_3 was from Buijsman et al. (1987). The NAPAP NH_3 emissions were too small compared with the Buijsman et al. (1987) estimate, judging by the human and cattle populations of the United States and Europe. Hence, we multiplied the NAPAP NH_3 emissions by 3.5, which gave a total reasonable compared with Seinfeld (1986, p. 15) and Buijsman et al. (1987). The emissions of CO were based on NO_x (Brost, 1988).

The total mass of reactive hydrocarbons was divided into 10 individual hydrocarbons using splitting factors derived from McRae et al. (1983), Derwent and Hov (1982), NAPAP (Toothman et al., 1984; Middleton, 1987), and the Electric Power Research Institute (Heisler et al., 1985; Middleton, 1987). Most of the mass was in higher alkanes, followed by aromatics and olefins (Table 3).

The emission inventories were reported on spatial scales smaller than those used here. Emission regions were determined within our modeled domain, and emissions within a region were summed. The regional average was used as input to the individual grid cells. The finer-scale emission data were thus spatially smoothed. The emission regions used were state and multistate regions in the United States, province and subprovince regions in Canada, and countries in Europe. There were a total of about 60 emission regions and 600 surface grid cells with emissions. Thus, emission regions averaged a reasonably well resolved 10 cells. Emissions were constant in time and apportioned to the lowest 500 m (4 model levels) to mimic results in Middleton (1987) and Chang et al. (1987). This gave a total of 2,400 cells with emissions. Brost et al. (1988a) showed that the Smolarkiewicz (1983) advection scheme used here produced a continuous plume that compared better with the plume from the highly accurate Prather (1986) advection scheme when the emissions were spatially smoothed. (A larger emission region produces larger plumes and puffs. If more grid cells span the advected shape, the concentration changes less between adjacent cells, and practically any advection scheme transports the shape more accurately.) McRae et al. (1982, 1983) also spatially smoothed their emissions to reduce the strain on the chemical integrator and advection scheme.

Table 2. *Anthropogenic emissions (Tg/year)*

Species	North America	Europe
SO_2	30	59
nitrogen as NO_2	26	20
volatile hydrocarbons	25	20
NH_3	3	6

Table 3. *Mass splitting factors for hydrocarbon emissions*

Species	Factor
acetaldehyde	0.016
formaldehyde	0.016
organic acid	0.007
butane + other alkanes	0.51
ethane	0.049
ethene	0.062
propene	0.032
butene	0.078
toluene	0.16
xylene	0.07

2.2.8. Deposition. Dry deposition of chemical species was estimated using the resistance formulation given in Walcek et al. (1986). The resistance depended on land use. The domain had 13 land use classes, whose characteristics were given in Anthes et al. (1987) and Walcek et al. (1986).

2.2.9. Initial and boundary conditions. The initial and boundary conditions were important to our analyses of the simulations. The boundary

concentrations were constant in time. We assumed artificially clean conditions to maximize the anthropogenically derived chemical signals (Table 4). There was no stratospheric source, that is, the initial and boundary conditions were constant in height. (NH_3 was an unimportant exception. It decreased with height.) We intended to isolate the O_3 produced by anthropogenic sources in these first numerical experiments. Here we concentrated on continental areas and regions influenced by continental plumes. These simulations might give accurate estimates of fluxes of S and N from North America to the Atlantic Ocean for the last two weeks of April 1982. Further tests are needed to decide how to handle stratospheric injection of O_3 and NO_x into the troposphere. Outside continents and continental plumes, we cannot simulate the chemistry well until we include stratospheric-tropospheric exchange. Thus, we did not consider the NO_x and O_3 budgets in detail here. In future work we will add more realistic initial and boundary conditions. We expect that more accurate estimates of ozone production and other chemical questions await further experience and model improvements.

Table 4. *Initial and boundary conditions*

Species	Concentration
SO_2	10 ppt
SO_4^{2-}	0 ppt
NO_2	20 ppt
NO	5 ppt
O_3	10 ppb
HNO_3	10 ppt
H_2O_2	1–0 ppb*
acetaldehyde	1 ppt
formaldehyde	0.1 ppb
organic peroxide (MHP)	0.1–0 ppb*
peroxyacetic acid	0.1–0 ppb*
organic acid	0 ppb
NH_3	0.5 ppb in PBL, 0.05 ppb aloft
N_2O_5	0 ppb
NO_3	0 ppb
butane + other alkanes	0.5 ppb
PAN	10 ppt
ethane	1 ppb
CO	120 ppb
ethene	0.6 ppb
propene	0.4 ppb
butene	0.2 ppb
toluene	0.3 ppb
xylene	0.3 ppb

* Decreases linearly with latitude.

2.2.10. Experiments. There were two chemical model experiments of 30 days duration. The "without cloud" experiment did not have vertical redistribution by clouds, wet scavenging by rain, or aqueous chemistry in clouds in the model chemistry and transport. Neither precipitating nor nonprecipitating clouds were included. The "with clouds" experiment used these processes by both kinds of clouds.

In other work, Brost and Chatfield (1988) have used the same meteorology and domain to test the effect of the cloud parameterizations in the simulation of radon. Simulated concentrations using this cloud transport parameterization agreed with radon observations near the surface over the Atlantic Ocean. At $z = 10$ km over North America, however, this cloud vertical transport was perhaps typical of the maximum that might be found during summer. Simulations with about half as much cloud transport (that is, they used precipitating cloud transport but did not use nonprecipitating cloud transport) gave the best agreement in the upper troposphere over land. Further work is needed to see whether this April had typical vertical and horizontal transport. Brost and Chatfield concluded that the most realistic parameterization of cloud transport was either the model with clouds used here or perhaps slightly less cloud transport.

3. Results

3.1. The approach to quasi-steady state

The total species mass in the modeled domain changed until there was a balance of gains and losses. The gains included mean transport from the lateral boundaries, emissions, and chemical production. The losses were mean lateral transport from the domain, chemical loss, dry deposition, and wet deposition.

A quasi-steady state (QSS) developed when the change in mass became small, say, less than a few per cent per day. (We expect short- and long-term meteorological and chemical fluctuations to prevent the total mass from becoming exactly constant. Hence we say quasi-steady state. The

reader should not confuse this with the quasi-steady state assumption of Hesstvedt et al., 1978, which we use for non-transported species.) The time required for relaxation to QSS differed for each species. These differences were significant and interesting. Because we only considered anthropogenic emissions, a small fraction of our surface area had emissions (21%). Only 6% of the grid cells and 0.7% of the simulated volume had emissions. A considerable time was required to transport these emissions over the modeled volume. If natural emissions increased the fraction of the simulated volume with sources, adding natural emissions might reduce the time scales for QSS found here. If there were a source in every grid cell, then the transport time would be unimportant, and local processes, such as photochemistry and deposition, would determine the time scale. For our domain, most of the sulfur emissions should be anthropogenic, but natural emissions should be more important for nitrogen. The lateral boundary conditions were clean so that emissions were the dominant sources of sulfur and nitrogen here. For most species, the relaxation to QSS was faster with clouds than without clouds.

Fig. 2 shows the temporal evolution of the domain-total mass of sulfur, total odd nitrogen, SO_2, PAN, SO_4^{2-}, and HNO_3. The mass is shown at 00 GMT on each day, so that Fig. 2 does not have diurnal effects. For many species the initial concentrations were constant throughout the domain (Table 4); hence, if the initial and final concentrations were comparable, the approximate average concentration could be inferred from the figures.

Clouds increased the amount of SO_4^{2-} and PAN. SO_4^{2-} increased because of aqueous conversion in fair-weather clouds (Brost, 1988). In a humidity-dependent fraction of each grid cell, these clouds were simulated to form for one hour and then to evaporate. When the fair-weather cloud evaporated, the new sulfate aerosol returned to the environment. PAN probably increased because precipitating clouds transported PAN and its precursors from the boundary layer to the free atmosphere where the lifetime of PAN was longer. All other species in Fig. 2 were reduced by clouds.

The mass of sulfur started near zero, and might have still been increasing at the end of a month. The small oscillations on the generally increasing trend had a period of 5–6 days and a meteorological source. Wet scavenging by clouds reduced the total mass of sulfur by 30%. The proportion of sulfur in SO_2 and SO_4^{2-} was drastically altered by clouds, particularly fair-weather clouds (Brost, 1988). The mass of SO_2 was reduced by 80% by the wet removal and aqueous phase conversion to SO_4^{2-}. Clouds produced large temporal changes in SO_2 mass; these changes were meteorologically induced by individual storms moving over the source regions. With clouds, QSS for SO_2 was reached within a remarkably short period of a few days. The SO_4^{2-} without clouds increased linearly with time because of gas-phase chemistry, but the changes with clouds were more irregular.

The mass of total odd nitrogen also increased most of the month, particularly in the absence of clouds. The largest mass of nitrogen was in HNO_3, and the second largest mass in PAN. The mass of PAN peaked on day 12 and then decreased, probably because of thermal decomposition as the average temperature increased throughout the simulated spring month. The total NO_x as nitrogen (not shown) increased about linearly at 1.0–1.3% per day, with the faster rate applying without clouds. This increase was consistent with the increase of total nitrogen (Fig. 2b) and the thermal decomposition of PAN. The mass of NO_x as nitrogen ranged from $1–1.7 \times 10^{10}$ g, so that 10–15% of the total odd nitrogen was in NO_x. Excursions of 10% above and below the mean were common. There was no consistent difference in NO_x between the two experiments.

Fig. 3 shows the temporal evolutions of O_3, HO, H_2O_2, HCHO, organic peroxide, and acetaldehyde. All species in this figure reached QSS faster than those in Fig. 2. Clouds increased the O_3 and HO. Clouds mixed species vertically, which increased the total O_3 in the domain for two reasons. First, photolysis rate constants increase with height. Second, because of nonlinear chemistry, the O_3 produced per NO_x often increases as NO_x decreases (Liu et al., 1987). The initial and boundary conditions of NO_x were 25 pptv. Outside the continental plumes, much of the atmosphere had less than a critical NO_x of 30 pptv (Fishman et al., 1979; Logan et al., 1981), so that O_3 was being destroyed. Cloud mixing in-

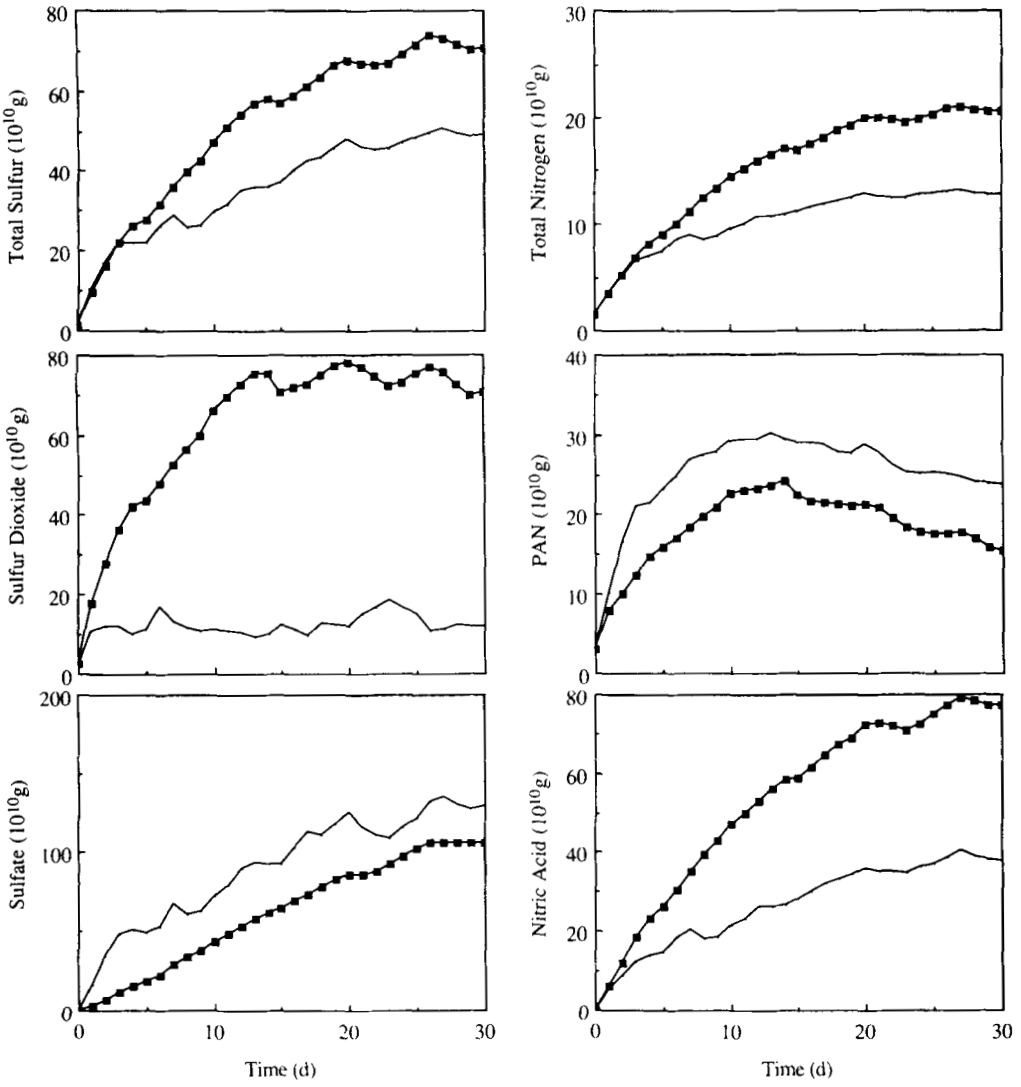

Fig. 2. The temporal evolution of the total mass of species in the domain. The filled squares are for the experiment without clouds and the solid lines for the experiment with clouds. The plotted points are valid at 00 GMT on each day, with day 0 corresponding to 1 April 1982.

creased the percentage volume of the model in which O_3 was being produced. The initial concentration of O_3 happened to be near the QSS concentration without clouds; thus, no time scale may be inferred from the behavior of O_3 without clouds.

Clouds decreased the H_2O_2 and organic peroxide. The simulated clouds produced large fluctuations in total HO, and, among all species, HO showed the largest percent change in total mass between experiments. HO_2 (not shown) reached a QSS faster than HO, within a few days, and then stayed constant to within a few percent. HO_2 also increased with clouds. This increased the chemical production of H_2O_2, but aqueous chemistry increased the loss of H_2O_2, so that with clouds the peroxide decreased.

The approach to QSS was particularly rapid for

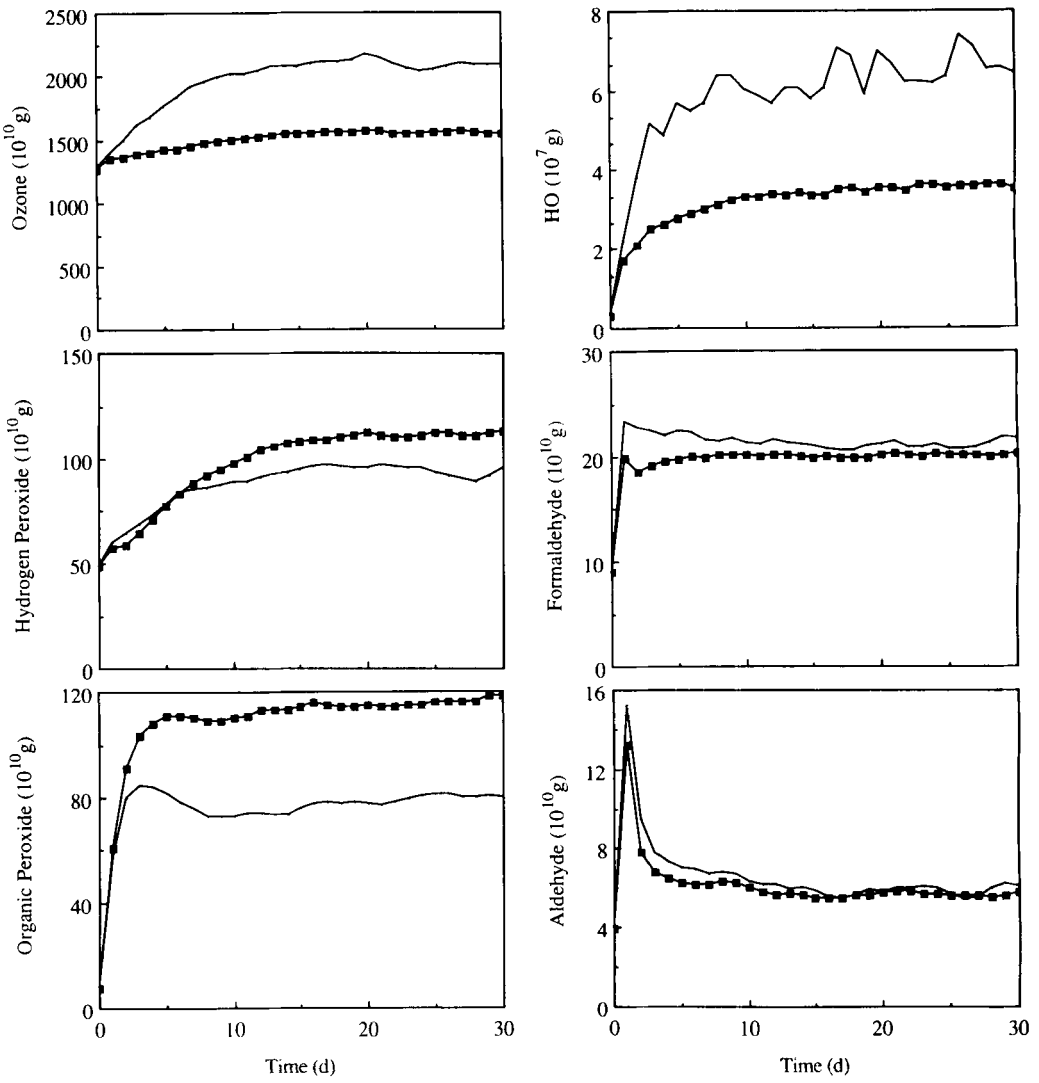

Fig. 3. The temporal evolution of the total mass of species in the domain. For HO, we picked the highest mass during each day. For all other species, the mass was chosen at 00 GMT on each day. See Fig. 2.

HCHO, faster than any other species, including species such as HO and butene. Clouds had a particularly small effect on HCHO. The final average concentration of HCHO was 0.25 ppb.

In tests using a separate model, the behavior of HCHO was simulated with a highly detailed inorganic and methane chemistry model (Kerr and Calvert, 1985). The 0-D model assumed no sources or sinks from processes other than chemical reactions. For the initial conditions used here, HCHO rose from the initial value to a steady state comparable to Fig. 3 in less than one day, and then remained constant for several days until NO_x depletion caused a slow downward drift. Thus, methane chemistry alone may explain HCHO in the background atmosphere.

In a smaller domain, Brost (1988) tested the uncertainty induced in concentrations of species by perturbations in meteorology, boundary conditions, and initial conditions. HCHO had the

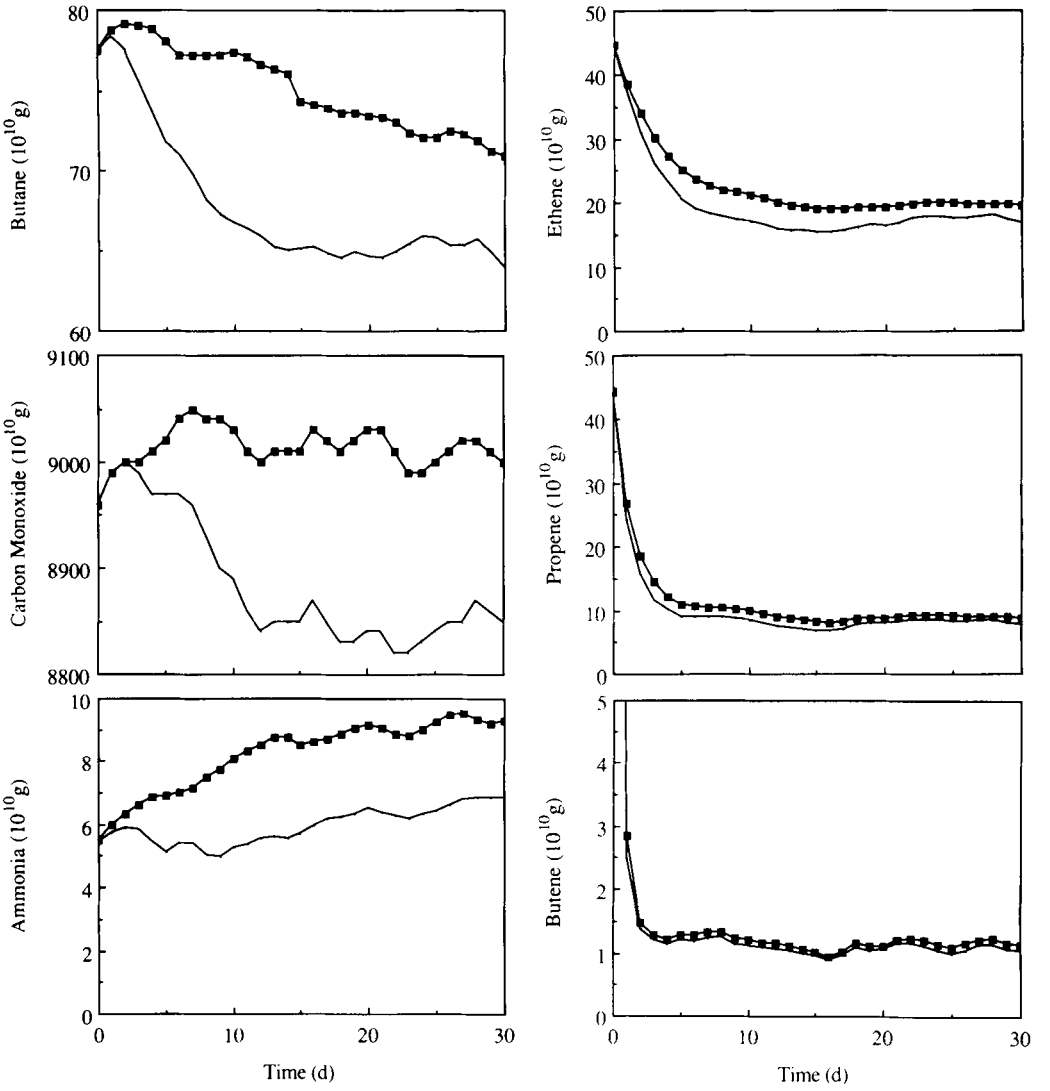

Fig. 4. The temporal evolution of the total mass of species in the domain. See Fig. 2.

smallest ratio σ_t/c_b, where σ_t was produced by changes in input conditions and was the standard deviation of the fluctuations horizontally about c_b, the horizontally averaged concentration.

Fig. 4 shows the temporal evolution of butane, ethene, CO, propene, NH_3, and butene. Note that the vertical axes for CO and butane do not include zero. Clouds decreased the total masses of all species in this figure. The behavior of CO was particularly interesting. Without clouds, the mass increased because of emissions. With clouds, the mass initially increased from emissions, but then decreased below the initial value. On day 11, a QSS was reached. Between days 6 and 11, there was a rapid decrease that could only have been produced by photochemistry and reaction with HO. Further work is needed to see if the concentration of HO was too large, and hence the loss of CO was abnormally large. Looking at the right-hand column, as the hydrocarbons became more reactive, the approach to QSS was faster and the effect of clouds was smaller. The initial

concentrations of ethene, propene, and butene were 0.6, 0.4, and 0.2 ppb, respectively. These were chosen based on clean air concentrations taken in the free atmosphere, west of the Rocky Mountains. The final average concentration of ethene (0.3 ppb) was a factor of two less than the initial. Propene was one fourth as much (0.1 ppb). Butene decreased twentyfold to 0.01 ppb. These final levels were partly maintained by lateral boundary conditions and not emissions. These three reactive hydrocarbons mainly persisted north of the polar front where the HO was low (shown later). The anthropogenic emissions could not maintain the initial levels of reactive hydrocarbons in the domain. Perhaps including natural emissions would significantly raise the average concentrations of reactive hydrocarbons. Most plant emissions are in summer as isoprene and alpha-pinene (Zimmerman 1979; Lamb et al., 1987). Isoprene should be lumped with butene in the Stockwell (1986) mechanism, and should substantially increase the butene concentration. Alpha-pinene should be lumped with butene or propene, with similar results. April, however, is before the maximum of natural emissions during the summer.

Generally, the species approached QSS more quickly with clouds because of higher winds aloft and because of the additional loss (or gain) introduced by clouds. Higher wind speeds moved species faster to the far corners of the domain and from the domain. This reduced the transport limitation in the convergence to QSS. Clouds also reduced the lifetime of soluble species, and increased the production of product species, such as sulfate. Only CO approached QSS slower with clouds, because clouds increased the HO, which slowly oxidized CO. Table 5 gives the e-folding time needed for 63% of the transition from the initial condition to the QSS. Based on these time scales, we only analyzed the last 15 days, when there was a QSS.

Table 5. *Time for adjustment to quasi-steady state*

Species	e-folding time (days)
total reactive nitrogen	7
O_3	6
H_2O_2	6
CO	6
ethene	3
propene	1.3
butene	<1
total sulfur	11
SO_2	4
SO_4^{2-}	12

3.2. *Effects of clouds*

Clouds have three important effects for atmospheric chemistry. First, photolysis rate constants increase above clouds and decrease below clouds (Madronich, 1987). Second, soluble species may enter cloud or rain drops, and then react in the aqueous phase or fall in rain drops to the surface of the earth. Third, clouds vigorously transport species vertically (Chatfield, 1982; Gidel, 1983; Chatfield and Crutzen, 1984; Cho et al., 1984; Isaac et al., 1984; Ritter, 1984; Ching and Alkezweeny, 1986; Kavassalis et al., 1986; Lyons et al. 1986; Niewiadomski, 1986; Walcek and Taylor, 1986; Dickerson et al., 1987; Pickering et al., 1988). In general, we found continental plumes without clouds, but sometimes the plumes were nonexistent or indistinct with clouds. In the remaining figures, the concentrations were averaged for the last 60 times, each separated by 6 h, for a total of 15 days.

The original pristine, background ozone was 10 ppb (Fig. 5a). There were continental plumes moving toward the northwest from North America and toward the south from Europe. Over North America, the peak concentrations were 67 ppb over southern California and 64 ppb over northern Florida. The large NO_x emissions depressed the O_3 level in central Europe. The European maxima were 80 ppb and higher.

In our simulations, anthropogenic emissions of nitrogen oxides and hydrocarbons increased the total ozone in the domain. In the nocturnal boundary layer, however, O_3 dry deposition and NO_x emission could sometimes combine to suppress the concentration of O_3 for $z < 100$ m. NO_x was emitted as NO, and this emission was simulated as constant in time, without the normal nocturnal minimum. At night, NO reacted with O_3 to produce NO_2, until either NO or O_3 disappeared. In shallow layers with a large emission of NO, the emitted NO sometimes significantly depleted the O_3. (In the real world, nighttime is a period of reduced mixing, and regions of higher concentrations of NO and O_3

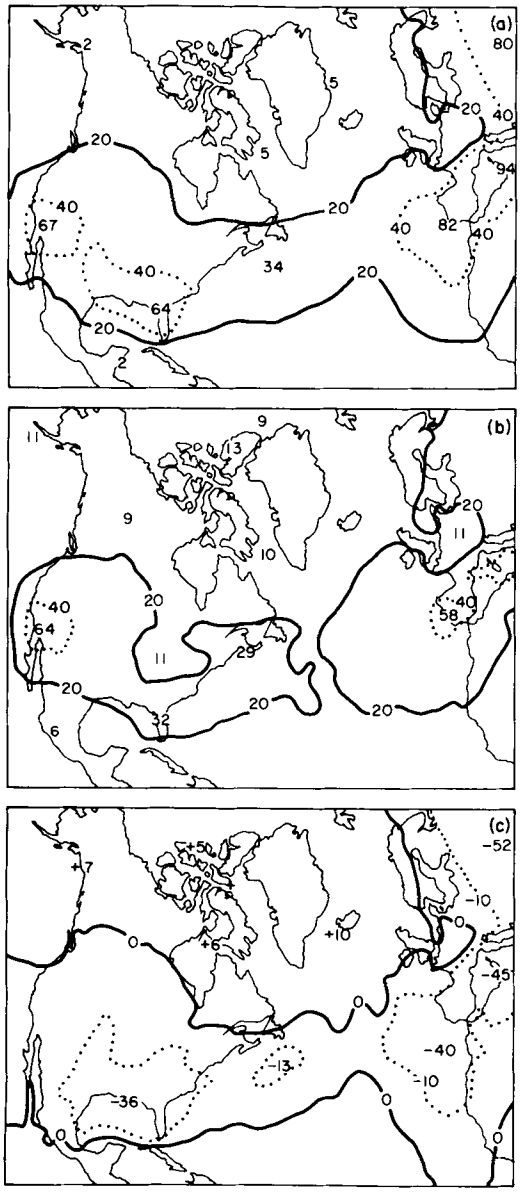

Fig. 5. For $z = 80$–160 m, we show O_3 in ppb averaged for the last 15 days of April. Panel (a) is for the experiment without clouds. Panel (b) for the experiment with clouds. Panel (c) shows the cloud minus no cloud values.

may be physically isolated, so that O_3 and NO coexist in pockets smaller than our grid.) During the day, the emission of NO was diluted in a much deeper PBL, and reaction of NO and O_3 could rarely reduce the O_3 in such an observable manner. In daytime, the photolysis of NO_2 rapidly regenerated both NO and O_3, which could then react to form NO_2, and a steady state could be reached. This cycle normally had little effect on O_3. Large effects on O_3 normally depended on other chemistry, involving CO and hydrocarbons, that shifted nitrogen between NO_2 and NO without affecting O_3. If the NO_x was below the critical level, the O_3 was depleted during the day; otherwise, the O_3 increased during the day, which was normal in polluted regions. Thus, the diurnally averaged O_3 was sometimes suppressed near source regions for $z < 100$ m, although it was always enhanced in the downstream plume and in the total for the domain. (The model probably exaggerated total ozone production, because it could not resolve subgrid scale plumes.) Without clouds, ozone and the emitted precursors that lead to ozone were largely confined to the PBL, say, $z < 2$ km during the day. The O_3 could become large in this confined layer. Clouds transported the ozone and its precursors vertically, which reduced the O_3 in the PBL, but increased the total O_3 in the domain.

The presence of clouds noticeably reduced the size and strength of the O_3 plumes in the PBL (Fig. 5b). Maxima were about halved; however, southern California was unaffected because of the lack of deep convection there. In the Ohio River Valley the concentration of O_3 was depressed below 20 ppb because of the strong NO_x sources and substantial cloud transport there.

In Fig. 5c, the regions with cloud-induced decreases in average ozone concentrations for $z = 80$–160 m were the United States, Europe, and the two plumes. North of the polar front, increases ranged up to 10 ppb at Iceland.

Fig. 6a shows the 15-day average ozone concentration with clouds minus that without clouds. The height was $z = 3.8$–4.9 km. Clouds raised the total amount of ozone, decreased the ozone in the PBL, and increased the ozone in the free atmosphere as in Fig. 6a. The maximum increase in Fig. 6a was 19 ppb.

HO and HO_2 are shown in Figs. 6b and 6c. Again, the values were for the PBL ($z = 80$–160 m). The HO concentration was high where the air was moist and polluted, especially at low latitudes. Thus, the concentrations were low in

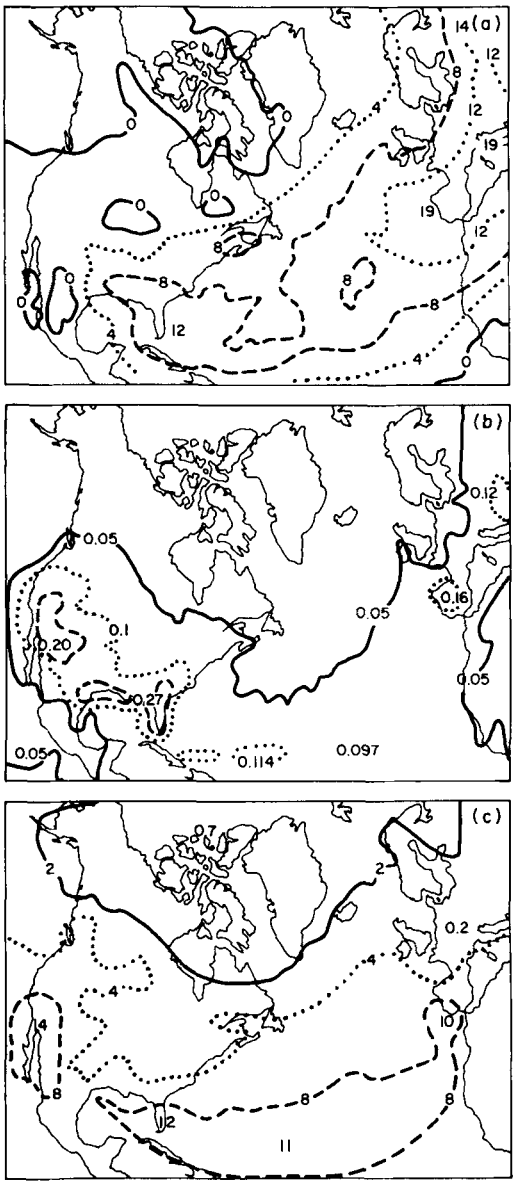

Fig. 6. All three panels have averages for the last 15 days of April. Panel (a) gives the cloud minus no cloud O_3 in ppb for $z = 3.8$–4.9 km. Panel (b) gives the HO in pptv with clouds for $z = 80$–160 m. Panel (c) has the HO_2 in pptv with clouds for $z = 80$–160 m.

northern Canada, Greenland, and the Sahara. The concentrations were high over the United States and southern Europe. The concentrations varied by at least a factor of 100. The largest values were over the Gulf states and Florida, as well as over Arizona and adjacent areas of Mexico. Spain also had high concentrations. The average position of the polar front over the Atlantic Ocean was probably reflected by the 0.05 pptv isoline. The largest values of HO_2 were in an arc from Baja California, across the Atlantic Ocean to Spain. Decreases near the southern boundary were probably not reliable, because they were dependent on values chosen for the boundary conditions.

Fig. 7 shows the 15-day average H_2O_2 in the PBL. Without clouds, the values decreased one hundredfold between the Gulf of Mexico and Alaska. The boundary condition varied linearly from 1 ppb in the south to 0 ppb in the north. The maxima were downwind of Europe, over west Africa, and downwind of the United States in the Gulf of Mexico. The decreases from these maxima to the boundaries were again not significant. With clouds (Fig. 7b), the concentrations were substantially reduced in the south and sometimes marginally increased in the north (Fig. 7c). The peak values decreased by two thirds.

The 15-day average CO in the PBL is given in Fig. 8. The boundary condition was 120 ppb. Without clouds, emissions raised the concentrations of CO to 263 ppb in the United States and 480 in Europe. The higher CO resulted in Europe for two reasons. First, the emission per area was higher in Europe than in the United States. Second, CO was confined to a PBL that was often shallower in Europe. For the same time period, Brost and Chatfield (1988) typically found the highest concentrations of radon near the surface in northern Europe and in northwestern Canada. Here the presence of clouds largely eradicated the North American and European plumes. With clouds, south of the polar front the values were all below the 120 ppb boundary value because of reaction with HO. Values were greater than 120 ppb in source regions and north of the polar front.

Finally, Fig. 9 shows the 15-day average ethene at three heights. Near the surface, the emissions were dominant (Fig. 9a). Maxima existed near Los Angeles, the northeastern United States, and central Europe. In the upper PBL ($z = 500$–800 m), the lowest values in Fig. 9b coincided with the highest levels of HO over the Atlantic Ocean (Fig. 6b). The increase toward the southern boundary was artificial. The highest values oc-

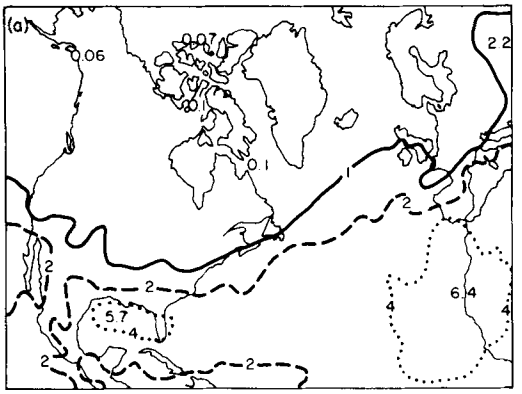

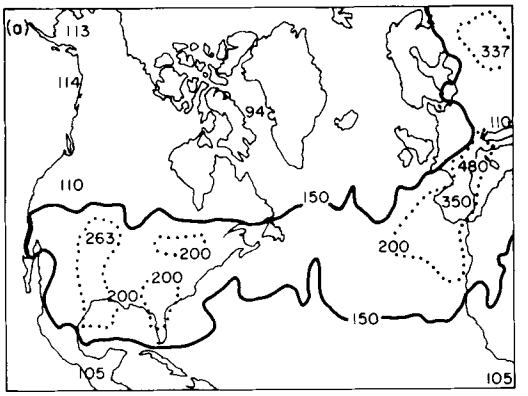

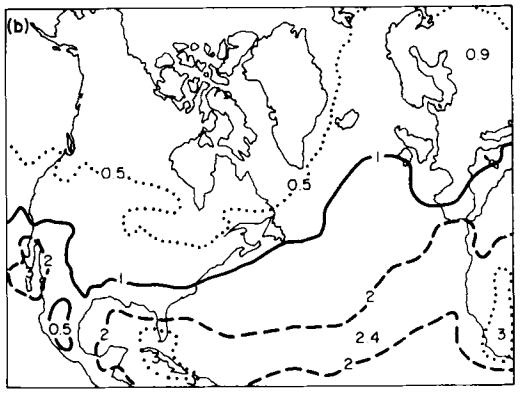

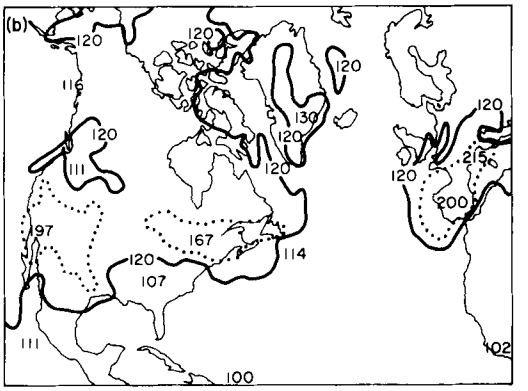

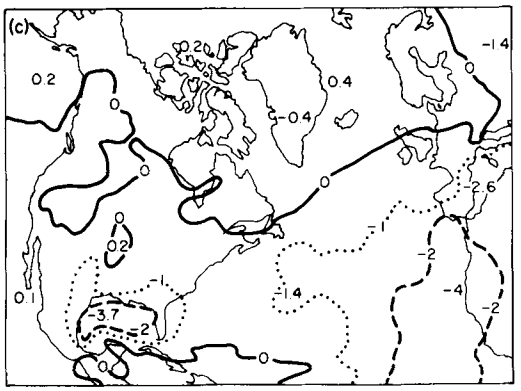

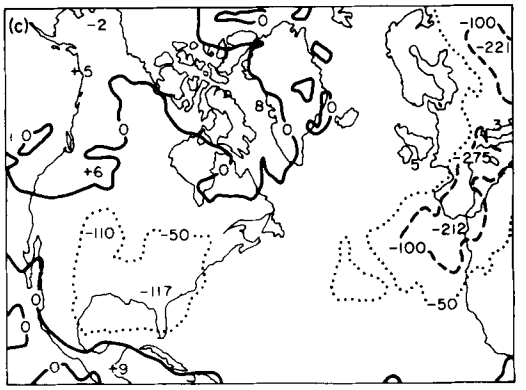

Fig. 7. Same as Fig. 5, except for H_2O_2.

Fig. 8. Same as Fig. 5, except for CO.

curred north of the polar front where there was little HO to oxidize the ethene. In the free atmosphere ($z = 3.8$–4.9 km), the same pattern was still evident (Fig. 9c). The high levels of ethene north of the polar front were at least partly the result of the boundary condition of 0.6 ppb ethene. This boundary condition and the levels north of the polar front might be too large, but HO was so low north of the front that the lifetime for ethene was long.

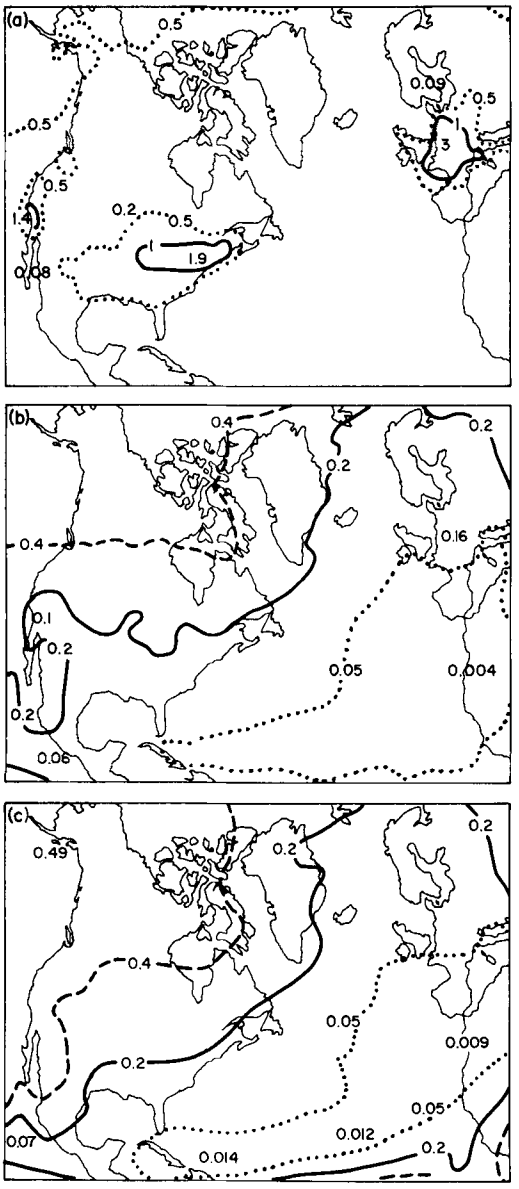

Fig. 9. Ethene (ppb), averaged for 15 days, at three heights: (a) 80–160 m, (b) 500–800 m, and (c) 3.8–4.9 km.

3.3. Horizontal fluxes of S and N from North America to the Atlantic Ocean

There are large anthropogenic emissions of sulfur and nitrogen from North America. Most of the emitted S and N is dry or wet deposited on North America and on the Atlantic Ocean (Galloway and Whelpdale, 1987). There have been many estimates of the fluxes of S and N from North America to the Atlantic Ocean (Table 6). The flux of S is probably better known than that of N. The species carrying the S and N depend on time of year and meteorological conditions. The S is largely emitted as SO_2, and undergoes a gas-phase oxidation to SO_4^{2-} during the day. The reaction is dependent on HO and hence sunlight, and is rapid during the summer, with several percent of the SO_2 oxidized every hour, and slow during the winter, a few tenths of a percent per hour. Aqueous reactions produce much higher conversion rates, but clouds are spatially and temporally intermittent. Qualitatively, we expect more of the flux of S to be in SO_2 during winter and less in summer. Likewise, the fraction in SO_4^{2-} should be larger during summer. Similarly, N is emitted largely as NO, which undergoes gas-phase conversion to HNO_3. Nitrogen can also be stored in PAN, which decomposes at high temperature. Also, nitric acid can form particulate nitrate. For N, the fraction in NO_x should probably be larger during winter, and the fraction in HNO_3 larger during summer. It is unclear whether the fraction in PAN should vary with season (Singh et al., 1985). Although PAN is more thermally stable at low temperature, in winter there is less photochemistry to create the PAN. We also do not know whether the fraction of N in nitrate aerosol depends on season. In comparing model simulations and data analyses for different seasons and meteorology, we expect differences in speciation and total flux.

Table 6 compares our model-simulated fluxes with other model simulations and with analyses based on data. Even if our 15-day period were perfectly simulated, the extrapolation from a single 15-day period to yearly fluxes might produce errors. (Among our five 3-day periods, the fluxes varied by about 50%). Researchers have analyzed observations in two ways to give fluxes. First, fluxes can be derived from climatological concentrations and air mass fluxes. Second, a few hours of observations taken during an intensive campaign of a few days duration can be extrapolated to yearly fluxes. Table 6 should tell us something about our model and perhaps about the analyses. Also, our simulations can fill in detail not found in the analyses.

Table 6. *Fluxes of sulfur and nitrogen from North America to the Atlantic Ocean*

Species	Reference	Flux of S (Tg/year) for each height range (km)				
		0–1.5	1.5–3.0	3.0–5.5	0–5.5	0–16
S in SO_2	MNC/MC[1]	2.9/1.1	1.5/0.2	1.1/0.2	5.5/1.4	6.0/1.8
	G84[2]	—	—	—	1.7	—
	T87[3]	2.1	0.21	0.36	2.7	—
S in SO_4^{2-}	MNC/MC[1]	0.5/0.4	1.1/0.9	1.3/2.2	2.9/3.4	3.4/7.1
	G84[2]	—	—	—	2.6	—
total S	MNC/MC[1]	3.4/1.5	2.6/1.0	2.4/2.2	8.4/4.8	9.4/8.9
	F86[4]	—	—	—	2.1	—
	B84[5]	—	—	—	3.0	—
	GW87[6]	—	—	—	3–4	—
	GW80[7]	—	—	—	4.3	—
	G84[2]	2.1	1.1	1.1	4.3	—
	SL86[8]	—	—	—	5.8	—

Species	Reference	Flux of N (Tg/year) for each height range (km)				
		0–1.5	1.5–3.0	3.0–5.5	0–5.5	0–16
N in NO_x	MNC/MC[1]	0.3/0.2	0.01/0.1	0.00/0.1	0.3/0.4	0.3/0.6
	G84[2]	—	—	—	2.7	—
N in HNO_3	MNC/MC[1]	0.7/0.2	0.8/0.2	0.9/0.6	2.4/1.0	2.9/1.9
N in NO_3^-	G84[2]	—	—	—	0.5	—
N in PAN	MNC/MC[1]	0.2/0.1	0.1/0.1	0.1/0.3	0.3/0.5	0.4/1.0
total N	MNC/MC[1]	1.1/0.5	0.9/0.4	1.0/0.9	3.0/1.8	3.6/3.6
	LD87[9]	—	—	—	0.5	—
	GW87[6]	—	—	—	0.8–1.2	—
	L83[10]	—	—	—	1.6	—
	B84[5]	—	—	—	1.6	—
	G84[2]	1.1	1.0	1.1	3.2	—

[1] Values simulated by model with no cloud transport/modeled values using cloud transport.
[2] Data analysis of Galloway et al. (1984).
[3] Data of Thornton et al. (1987).
[4] Data analysis by Fay et al. (1986).
[5] Data analysis by Bischoff et al. (1984).
[6] Data analysis by Galloway and Whelpdale (1987).
[7] Data analysis by Galloway and Whelpdale (1980).
[8] Lagrangian modeling by Shannon and Lesht cited by Galloway and Whelpdale (1987).
[9] Data of Luke and Dickerson (1987).
[10] Data analysis and modeling by Logan (1983).

Thornton et al. (1987) observed SO_2 concentrations during the January 1986 phase of the Western Atlantic Ocean Experiment, WATOX-86. Stunder et al. (1987) argued that the horizontal, atmospheric mass fluxes during the four days of WATOX-86 were typical of January, and perhaps much of the winter. In all height ranges, the SO_2 fluxes of Thornton et al. were between our simulated values for with and without clouds. It seems reasonable that our model simulations without clouds had too much SO_2. Our simulations with clouds had less SO_2 than January observations because of greater gas-phase oxidation in April.

Galloway et al. (1984) provided the most complete analysis of speciation and of latitudinal and height variations. Galloway et al. (1984) constructed climatological vertical profiles of the sulfur and nitrogen species from observations. Using climatological winds, they calculated

fluxes crossing the eastern boundary of North America between 25 and 60°N (Table 6). They concluded that 75% of the fluxes occurred between 33 and 48°N. The fluxes were broken up into three height intervals below 5.5 km (Table 6). (Normally data analyses have ignored or found insignificant fluxes above 5.5 km, contrary to our model results with clouds.) Sulfur dioxide carried 40% of the sulfur flux, and sulfate carried 60%. (For WATOX-86, Whelpdale et al. (1987) found 30% of the S in SO_4^{2-}. It is reasonable that sulfate should carry a smaller percent of S in January than in the annual average.)

The sulfur speciation is the same in our model and the analysis (Table 6). For $z < 5.5$ km and the total sulfur flux, our model with clouds agreed well with the Galloway et al. (1984) analysis. The agreement was excellent everywhere except for $z = 3$–5.5 km. The largest difference between our model simulations was in the SO_2 flux, where the model with clouds gave good agreement with the analysis, but the without cloud value was about three times the analysis. Without clouds our simulated sulfur flux was largely in SO_2 (64%); with clouds, our flux was predominantly SO_4^{2-} (80%). In our two simulations, the percentages of the total fluxes in SO_2 or SO_4^{2-} bracketed the Galloway et al. (1984) respective analyzed percentages.

Often substantial fluxes extended higher in our simulations than in any analyses (i.e., for $z > 5.5$ km). Without clouds, our fluxes in the upper troposphere might have been dominated by the upstream boundary conditions, but, with cloud transport, the fluxes should not have been. The total tropospheric S fluxes in our two simulations were almost identical, despite differences in the speciation and height distribution.

More uncertainty exists in the analysis of N fluxes than in the analysis of S fluxes. Because the emission of N is less well known that that of S, our simulated fluxes were also more uncertain. For $z < 5.5$ km, our total flux of nitrogen without clouds agreed almost exactly with the Galloway et al. (1984) analysis, but this agreement is perhaps misleading. The speciation differed greatly in our simulations and the analysis. The predominance of NO_x in the N flux is probably not accepted now (Galloway and Whelpdale, 1987). (For WATOX-86, Whelpdale et al. (1987) found that particulate nitrate accounted for 40% of the total nitrate.) Our model had sufficiently active chemistry (springtime HO), so that NO_x was substantially converted to HNO_3. Our modeled fluxes were largely nitric acid vapor (50–80%), with NO_x contributing 10–20%. Our model did not include nitrate aerosol, much of which would probably come from nitric acid vapor. Our model also had a substantial flux of nitrogen in PAN (10–30%); this flux increased with height, and might have been sensitive to upstream boundary conditions. With clouds, our total flux of nitrogen for $z < 5.5$ km was only 60% of the Galloway et al. (1984) analyzed flux, but this analyzed flux was large compared to other analyses. The tropospheric total fluxes of N for both our model simulations were again practically identical.

The estimates of total fluxes for $z < 5.5$ km have varied from 2.1–5.8 Tg S/year and 0.5–3.2 Tg N/year. Galloway and Whelpdale (1987) reviewed other work and probably gave the best estimate for the total fluxes: 3–4 Tg/year for S and 0.8–1.2 Tg/year for N. Model studies have tended to estimate larger fluxes. A Lagrangian model study found a flux of 5.8 Tg S/year (Galloway and Whelpdale, 1987). Our modeled fluxes were also on the high side of the ranges of analyzed data for $z < 5.5$ km. For the total troposphere, our modeled values were about twice the best estimates. For North America, Galloway and Whelpdale (1987) cited total emissions of 11.7 Tg S/year and 4.5 Tg N/year, which are 78% and 57% of our total emissions. If we scaled our total fluxes downward based on their emissions, our simulated fluxes below 5.5 km, using cloud transport, would have been about 3.7 Tg S/year and 1.0 Tg N/year, both within the Galloway and Whelpdale (1987) ranges.

Our large simulated fluxes above 5.5 km might have been partly produced by lateral boundary conditions. Also, perhaps, our simulated period was atypical. It is also possible that the analyses have missed a significant flux of S and N above 5.5 km.

4. Conclusions

We reached several conclusions in this study.

(1) The simulations with cloud transport were more realistic than those without cloud transport.

(2) Two weeks were required to develop a quasi-steady state (QSS) in this domain. Because we are modeling about 40% of a hemisphere, two weeks seemed consistent with a one month mixing time for an entire hemisphere. The species that required the longest time to reach QSS were product acids, SO_4^{2-} and HNO_3, and total sulfur and total nitrogen.

(3) Clouds made the atmosphere more oxidizing by increasing the total mass of HO and O_3.

(4) In the PBL, there were horizontal plumes over the Atlantic Ocean. We could intermittently identify (instantaneous) blobs of species from North America and Europe (not shown). In a 15-day average, the European plume was larger and stronger, probably because it was more confined to the PBL, and had less cloud transport from the PBL. It was easier to identify plumes without clouds, because clouds could disrupt or eradicate the plumes.

(5) HO was high in polluted and humid regions. Some reactive hydrocarbons could only persist north of the polar front where HO was low. South of the polar front, anthropogenic emissions were insufficient to maintain significant clean air concentrations of the most reactive hydrocarbons.

(6) For $z < 5.5$ km, the fluxes of N and S from North America to the Atlantic Ocean were slightly higher than the best estimate from Galloway and Whelpdale (1987). They estimated 3–4 Tg S/year and 0.8–1.2 Tg N/year, whereas we extrapolated from our 15-day period and found 4.8 Tg S/year and 1.8 Tg N/year, when we used cloud transport. Our calculations were, however, within the scatter of previous analyses. We differed from data analyses largely because we found as much flux above 5.5 km as below. Despite large differences in speciation and height variation, both simulations gave almost identical total tropospheric fluxes of S and N. Using cloud transport, 59% of the sulfur and 46% of the nitrogen emitted to the North American atmosphere were advected eastward to the atmosphere above the Atlantic Ocean. These fractions were about twice the 25–35% for S and 15–25% for N found by Galloway and Whelpdale (1987).

(7) The peak horizontally averaged vertical eddy diffusivities in the PBL were 100–400 $m^2 s^{-1}$. At any location, the largest values could reach 4000 $m^2 s^{-1}$.

This work emphasized the importance of clouds so much that Brost and Chatfield (1988) tested our cloud parameterization by simulating radon for this domain and meteorology. In addition, we wish to add natural emissions to find the effect on O_3. Also, we must add more realistic initial and boundary conditions, as well as a stratosphere. Finally, we intend to simulate the WATOX-86 period and make detailed comparisons of simulated and observed concentrations.

5. Acknowledgements

We thank R. A. Anthes and Y.-H. Kuo for access to their mesoscale modeling system.

REFERENCES

Anthes, R. A. and Warner, T. T. 1978. Development of hydrostatic models suitable for air pollution and other mesometeorological studies. *Mon. Wea. Rev. 106*, 1045–1078.

Anthes, R. A., Hsie, E.-Y. and Kuo, Y.-H. 1987. *Description of the Penn State/NCAR mesoscale model version 4 (MM4)*. NCAR technical note NCAR/TN-282 + STR, National Center for Atmospheric Research, P.O. Box 3000, Boulder, CO 80307, 66 pp.

Bischoff, W. D., Patterson, V. L. and McKenzie, F. T. 1984. Geochemical mass balance for sulfur- and nitrogen-bearing components: Eastern United States. In: *Geological aspects of acid deposition* (ed. O. P. Bricker). Acid Precipitation Series, 7. Boston: Butterworth, 1–20.

Blackadar, A. K. 1976. Modeling the nocturnal boundary layer. *Preprints of the 3rd Symposium on Atmospheric Turbulence, Diffusion, and Air Quality*. Rayleigh, NC, 19–22 October 1976, Amer. Meteor. Soc., Boston, 46–49.

Blackadar, A. K. 1979. High resolution models of the planetary boundary layer. In: *Advances in Environmental Sciences and Engineering, 1, No. 1* (eds. Pfafflin and Ziegler). New York: Gordon and Breach Sci Pub., 50–85.

Brost, R. A. and Wyngaard, J. C. 1978. A model study of the stably stratified planetary boundary layer. *J. Atmos. Sci. 35*, 1427–1440.

Brost, R. A. 1988. The sensitivity to input parameters of atmospheric concentrations simulated by a

regional scale chemical model. *J. Geophys. Res. 93*, 2371–2387.

Brost, R. A. and Chatfield, R. B. 1988. Transport of radon in a three-dimensional synoptic scale model. *J. Geophys. Res. 93*, in press.

Brost, R. A., Haagenson, P. L. and Kuo, Y.-H. 1988a. The effect of diffusion on tracer puffs simulated by a regional scale Eulerian model. *J. Geophys. Res. 93*, 2389–2404.

Brost, R. A., Haagenson, P. L. and Kuo, Y.-H. 1988b. Eulerian simulation of tracer distribution during CAPTEX. *J. Appl. Meteor. 27*, 579–593.

Buijsman, E., Maas, H. F. M. and Asman, W. A. H. 1987. Anthropogenic NH_3 emissions in Europe. *Atmos. Environ. 21*, 1009–1022.

Businger, J. A., Wyngaard, J. C., Izumi, Y. and Bradley, E. F. 1971. Flux profile relationships in the atmospheric surface layer. *J. Atmos. Sci. 28*, 181–189.

Carmichael, G. R. and Peters, L. K. 1984a. An Eulerian transport/transformation/removal model for SO_2 and sulfate–I. Model development. *Atmos. Environ. 18*, 937–951.

Carmichael, G. R. and Peters, L. K. 1984b. An Eulerian transport/transformation/removal model for SO_2 and sulfate–II. Model calculation of SO_x transport in the eastern United States. *Atmos. Environ. 18*, 953–967.

Chang, J. S. 1985. *The NCAR regional acid deposition model.* NCAR technical note NCAR/TN-256 + STR, National Center for Atmospheric Research, P.O. Box 3000, Boulder, CO 80307, 178 pp.

Chang, J. S. 1986. *Preliminary evaluation studies with the regional acid deposition model* (RADM). NCAR technical note NCAR/TN-265 + STR, National Center for Atmospheric Research, P.O. Box 3000, Boulder, CO 80307, 202 pp.

Chang, J. S., Brost, R. A., Isaksen, I. S. A., Madronich, S., Middleton, P., Stockwell, W. R. and Walcek, C. J. 1987. A three-dimensional Eulerian acid deposition model: Physical concepts and model formulation. *J. Geophys. Res. 92*, 14,681–14,700.

Chatfield, R. B. 1982. Remote tropospheric SO_2: *Cloud transport of reactive sulfur emissions.* Ph.D. thesis, Colo. State University, Ft. Collins, CO 80523, U.S.A.

Chatfield, R. B. and Crutzen, P. J. 1984. Sulfur dioxide in remote oceanic air: Cloud transport of reactive precursors. *J. Geophys. Res. 89*, 7111–7132.

Ching, J. K. S. and Alkezweeny, A. J. 1986. Tracer study of vertical exchange by clouds. *J. Clim. Appl. Meteorol. 25*, 1702–1711.

Cho, H. R., Iribarne, J. V., Grabenstetter, J. E. and Yam Y. T. 1984. Effects of cumulus cloud systems on the vertical distribution of air pollutants. In: *The meteorology of acid deposition* (ed. P. J. Samson). Air Pollution Control Association, Pittsburgh, PA, 127–139.

Derwent, R. G. and Hov, O. 1982. The potential for secondary pollutant formation in the atmospheric boundary layer in a high pressure situation over England. *Atmos. Environ. 16*, 655–665.

Dickerson, R. R., Huffman, G. J., Luke, W. T., Nunnermacker, L. J., Pickering, K. E., Leslie, A. C. D., Lindsey, C. G., Slinn, W. G. N., Kelley, T. J., Daum, P. H., Delany, A. C., Greenberg, J. P., Zimmerman, P. R., Boatman, J. F., Ray, J. D. and Stedman, D. H. 1987. Thunderstorms: An important mechanism in the transport of air pollutants. *Science 235*, 460–465.

Duce, R. A., Cicerone, R., Davis, D., Delwiche, C. C., Dickinson, R., Harriss, R., Hicks, B., Lenschow, D., Levy, H. II, Liu, S., McElroy, M., Mohnen, V., Niki, H. and Prospero, J. 1984. *Global tropospheric chemistry: a plan for action.* ISBN 0-309-03481-7. Washington, D.C.: National Academy Press.

Fay, J. A., Kumar, S. and Golomb, D. 1986. Annual and semiannual anthropogenic sulfur budget for eastern North America. *Atmos. Environ. 20*, 1497–1500.

Fishman, J., Solomon, S. and Crutzen, P. J. 1979. Observational and theoretical evidence in support of a significant in-situ photochemical source of tropospheric ozone. *Tellus 31*, 432–446.

Galloway, J. N. and Whelpdale, D. M. 1980. An atmospheric sulfur budget for eastern North America. *Atmos. Environ. 14*, 409–417.

Galloway, J. N., Whelpdale, D. M. and Wolff, G. T. 1984. The flux of S and N eastward from North America. *Atmos. Environ. 18*, 2595–2607.

Galloway, J. N. and Whelpdale, D. M. 1987. WATOX-86 overview and western north Atlantic Ocean S and N atmospheric budgets. *Global Biogeochemical Cycles 1*, 261–281.

Gidel, L. T. 1983. Cumulus cloud transport of transient tracers. *J. Geophys. Res. 88*, 6587–6599.

Heisler, S. L., Young, J., Lurmann, F., Hayden, P., Collins, H., Collins, J., Yeransian, T., Kringel, D. and Hay, G. 1985. The EPRI 1982 national air pollutant emissions inventory. *Proceedings, Air Pollution Control Association, 78th Annual Meeting*, Detroit, MI.

Hesstvedt, E., Hov, O. and Isaksen, I. S. A. 1978. Quasi-steady state approximations in air pollution modeling: comparison of two schemes for oxidant prediction. *Int. J. Chem. Kinetics 10*, 971–994.

Hov, O., Becker, K. H., Builtjes, P., Cox, R. A. and Kley, D. 1986. Evaluation of the photoxidants-precursor relationship in Europe. *Air pollution research report 1*, Commission of the European Communities, 122 pp.

Isaac, G. A., Joe, P. L. and Summers, P. W. 1984. The vertical transport and redistribution of pollutants by clouds. In: *The meteorology of acid deposition* (ed. P. J. Samson). Air Pollution Control Association, Pittsburgh, PA, 496–512.

Jacob, D. J., Prather, M. J., Wofsy, S. C. and McElroy, M. B. 1987. Atmospheric distribution of ^{85}Kr simulated with a general circulation model. *J. Geophys. Res. 92*, 6614–6626.

Joseph J. H., Wiscombe, W. J. and Weinman, J. A.

1976. The delta-Eddington approximation for radiative flux transfer. *J. Atmos. Sci. 33*, 2452–2458.

Kavassalis, T. A., Melo, O. T., Iribarne, J. V. and Cho, H. R. 1986. Cloud microphysics and acid rain formation in frontal circulations. In: *Meteorology of acid deposition* (eds. J. Laznow and G. J. Stensland). Air Pollution Control Association, Pittsburgh, PA, 278–301.

Kerr, J. A. and Calvert, J. G. 1985. *Chemical transformation modules for eulerian acid deposition models. Vol. 1: The gas-phase chemistry*. U.S. Environmental Protection Agency Report, Interagency Agreement No. DW930237-01-0, National Center for Atmospheric Research, Boulder, CO 80307.

Lamb, R. G. 1982. *A regional scale (1000 km) model of photochemical air pollution. Part 1: Theoretical formulation*. Office of Research and Development, Environmental Sciences Research Laboratory, U.S. Environmental Protection Agency, Research Triangle Park, NC 27711.

Lamb, T. G. 1983. *A regional scale (1000 km) model of photochemical air pollution. Part 2: Input processor network design*. Office of Research and Development, Environmental Sciences Research Laboratory, U.S. Environmental Protection Agency, Research Triangle Park, NC 27711.

Lamb, R. G. 1985. *A regional scale (1000 km) model of photochemical air pollution. Part 3: Tests of numerical algorithms*. Office of Research and Development, Environmental Sciences Research Laboratory, U.S. Environmental Protection Agency, Research Triangle Park, NC 27711.

Lamb, B., Guenther, A., Gay, D. and Westberg, H. 1987. A national inventory of biogenic hydrocarbon emissions. *Atmos. Environ. 21*, 1695–1705.

Levy, H. II, Mahlman, J. D. and Moxim, W. J. 1982. Tropospheric N_2O variability. *J. Geophys. Res. 87*, 3061–3080.

Levy, H. II, Mahlman, J. D., Moxim, W. J. and Liu, S. C. 1985. Tropospheric ozone: The role of transport. *J. Geophys. Res. 90*, 3753–3772.

Liu, S. C., Trainer, M., Fehsenfeld, F. C., Parrish, D. D., Williams, E. J., Fahey, D. W., Hubler, G. and Murphy, P. C. 1987. Ozone production in the rural troposphere and the implications for regional and global ozone distributions. *J. Geophys. Res. 92*, 4191–4207.

Logan, J. A., Prather, M. J., Wofsy, S. C. and McElroy, M. B. 1981. Tropospheric chemistry: A global perspective. *J. Geophys. Res. 86*, 7210–7254.

Logan, J. A. 1983. Nitrogen oxides in the troposphere: Global and regional budgets. *J. Geophys. Res. 88*, 10,758–10,807.

Luke, W. T. and Dickerson, R. R. 1987. The flux of reactive nitrogen compounds from eastern North America to the western Atlantic Ocean. *Global Biogeochemical Cycles 2*, 329–343.

Lyons, W. A., Calby, R. H. and Keen, C. S. 1986. The impact of mesoscale convective systems on regional visibility and oxidant distribution during persistent elevated pollution episodes. *J. Clim. Appl. Meteorol. 25*, 1518–1531.

Madronich, S. 1987. Photodissociation in the atmosphere. I: Actinic flux and the effects of ground reflections and clouds. *J. Geophys. Res. 92*, 9740–9752.

Mahlman, J. D. and Moxim, W. J. 1978. Tracer simulation using a global general circulation model: Results from a midlatitude instantaneous source experiment. *J. Atmos. Sci. 35*, 1340–1374.

Mahlman, J. D., Levy II, H. and Moxim, W. J. 1980. Three-dimensional tracer structure and behavior as simulated in two ozone precursor experiments. *J. Atmos. Sci. 37*, 655–685.

Malone, R. C., Auer, L. H., Glatzmaier, G. A., Wood, M. C. and Toon, O. B. 1986. Nuclear winter: Three-dimensional simulations including interactive transport, scavenging, and solar heating of smoke. *J. Geophys. Res. 91*, 1039–1053.

McRae, G. J., Goodin, W. R. and Seinfeld, J. H. 1982. Development of a second generation mathematical model for urban air pollution—I. Model formulation. *Atmos. Environ. 16*, 679–696.

McRae, G. J., Goodin, W. R. and Seinfeld, J. H. 1983. Development of a second generation mathematical model for urban air pollution–II. Evaluation of model performance. *Atmos. Environ. 17*, 501–522.

Middleton, P. 1987. Analysis of emission databases for regional models. *Atmos. Environ. 21*, 1497–1509.

Moeng, C.-H. and Wyngaard, J. C. 1984. Statistics of conservative scalars in the convective boundary layer. *J. Atmos. Sci. 21*, 3161–3169.

Niewiadomski, M. 1986. A passive pollutant in a three-dimensional field of convective clouds: Numerical simulations. *Atmos. Environ. 20*, 139–145.

Pickering, K. E., Dickerson R. R., Huffman, G. J., Boatman, J. F. and Schanot, A. 1988. Trace gas transport in the vicinity of frontal convective clouds. *J. of Geophys. Res. 93*, 759–773.

Prather, M. J. 1986. Numerical advection by conservation of second-order moments. *J. of Geophys. Res. 91*, 6671–6681.

Prather, M. J., McElroy, M., Wofsy, S., Russell, G. and Rind, D. 1987. Chemistry of the global troposphere: fluorocarbons as tracers of air motion. *J. of Geophys. Res. 92*, 6579–6613.

Richtmyer, R. D. 1957. *Difference methods for initial-value problems*. New York: Interscience, 283 pp.

Ritter, J. A. 1984. The determination of cloud base mass flux and the vertical redistribution of a conservative tracer. In: *The Meteorology of acid deposition* (ed. P. J. Samson). Air Pollution Control Association, Pittsburgh, PA, 177–188.

Seinfeld, J. H. 1986. *Atmospheric Chemistry and Physics of Air Pollution*. New York: John Wiley, 738 pp.

Singh, H. B., Salas, L. J., Ridley, B. A., Shetter, J. D., Donahue, N. M., Fehsenfeld, F. C., Fahey, D. W., Parrish, D. D., Williams, E. J., Liu, S. C., Hubler, G.

and Murphy, P. C. 1985. Relationship between peroxyacetyl nitrate and nitrogen oxides in the clean troposphere. *Nature 318*, 347–349.

Smolarkiewicz, P. K. 1983. A positive definite advection scheme with small implicit diffusion. *Mon. Wea. Rev. 111*, 479–486.

Smolarkiewicz, P. K. 1984. A fully multidimensional positive advection scheme with small implicit diffusion. *J. Comp. Phys. 54*, 325–362.

Smolarkiewicz, P. K. and Clark, T. L. 1986. The multidimensional positive definite advection transport algorithm: Further development and applications. *J. Comp. Phys. 67*, 396–438.

Stockwell, W. R. 1986. A homogeneous gas phase mechanism for use in a regional acid deposition model. *Atmos. Environ. 20*, 1615–1632.

Stunder, B. J. B., Artz, R. S. and Rolph, G. D. 1987. WATOX meteorological overview for January 1986 WP-3D aircraft intensive. *Global Biogeochemical Cycles 1*, 283–295.

Thornton, D. C., Bandy, A. R. and Driedger, A. R. III 1987. Sulfur dioxide over the western Atlantic Ocean. *Global Biogeochemical Cycles 1*, 317–328.

Toothman, D. A., Yates, J. C. and Sabo, E. J. 1984. Status report on the development of the NAPAP emission inventory for the 1980 base year and the summary of preliminary data. *EPA-600/7-84-091*.

van Dop, H. and DeHaan, B. J. 1983. Mesoscale air pollution dispersion modeling. *Atmos. Environ. 17*, 1449–1456.

Venkatram, A. and Karamchandani, P. 1986. Source-receptor relationships, a look at acid deposition modeling. *Environ. Sci. Technol. 20*, 1084–1091.

Voldner, E. C., Shah, Y. and Whelpdale, D. M. 1980. A preliminary Canadian emissions inventory for sulfur and nitrogen oxides. *Atmos. Environ. 14*, 419–428.

Walcek, C. J. and Taylor, G. R. 1986. A theoretical method for computing vertical distributions of acidity and sulfate production within growing cumulus clouds. *J. Atmos. Sci. 43*, 339–355.

Walcek, C. J., Brost, R. A., Chang, J. S. and Wesely, M. L. 1986. SO_2, sulfate and HNO_3 deposition velocities computed using regional landuse and meteorological data. *Atmos. Environ. 20*, 949–964.

Whelpdale, D. M., Keene, W. C., Hansen, A. D. A. and Boatman J. 1987. Aircraft measurements of sulfur, nitrogen, and carbon species during WATOX-86. *Global Biogeochemical Cycles 1*, 357–368.

Wyngaard, J. C. and Brost, R. A. 1984. Top-down and bottom-up diffusion of a scalar in the convective boundary layer. *J. Atmos. Sci. 41*, 102–112.

Zhang, D.-L. and Anthes, R. A. 1982. A high-resolution model of the planetary boundary layer-sensitivity tests and comparisons with SESAME-79 data. *J. Appl. Meteor. 21*, 1595–1609.

Zimmerman, P. R. 1979. Testing of hydrocarbon emissions from vegetation, leaf litter and aquatic surfaces, and development of a methodology for compiling biogenic emission inventories. Final Report. *Report Number EPA-450/4-79-004*, United States Environmental Protection Agency, Office of Air Quality, Planning and Standards, Research Triangle Park NC 27711. Available from Library Services Office (MD-35) and as PB-296 070 from National Technical Information Service, Springfield, VA 22161, USA.